Combination of Solid State and Electrochemical Impedance Spectroscopy to Explore Effects of Porosity in Sol-Gel Derived $BaTiO_3$ Thin Films

Joshua Whittam,[a] Andrew L. Hector,[a,*] Christopher Kavanagh,[b] John R. Owen[a] and Gillian Reid[a]

[a] Chemistry, University of Southampton, Highfield, Southampton SO17 1BJ, UK. Email A.L.Hector@soton.ac.uk

[b] Deregallera Ltd, Unit 2 De Clare Court, Pontygwindy Industrial Estate, Caerphilly CF83 3HU, UK

$BaTiO_3$ thin films were deposited onto polycrystalline Pt using a dip-coating technique, with annealing temperatures of 750 to 900 °C. To avoid film imperfections such as cracking or regions of zero $BaTiO_3$ coverage (pinholes), key conditions, including aging periods, water content, and spin velocities, were refined to produce a pinhole free, uniform films with some porosity. Whilst those coated a single time short circuited during electrical characterization, this could be avoided in films produced by multiple coating cycles. The relative permittivity of a 600 nm $BaTiO_3$ film was measured at 290 by fitting solid state impedance data in the frequency range 100 Hz to 1 MHz. Electrochemical impedance with an aqueous electrolyte allowed evaluation of the porosity, which remained fairly constant between one and five coating cycles. Using this method it was possible to estimate the relative permittivity of the $BaTiO_3$ itself as 374 and hence to evaluate the increase in the relative permittivity that could be achievable by minimizing porosity.

Introduction

Titanate perovskites such as lead zirconate titanate ($PbZr_xTi_{1-x}O_3$), strontium titanate ($SrTiO_3$) and barium titanate ($BaTiO_3$) are workhorse electroceramic materials. They have various important electrical properties, including reports of relative permittivities of 273 (1 kHz, 500 nm),[1] 475 (100 kHz, 600 nm)[2] and 630 (1 kHz, 380 nm),[3] respectively, in thin films. Applications include high charge-density capacitors and dynamic random access memories.[4] Capacitors based on such electroceramics are ubiquitous energy storage devices in electronics applications, e.g. in surface-mounted multilayer capacitors and in larger capacitance rolled devices.[5,6]

In most applications electroceramic materials are prepared by conventional powder processing methods at high temperature. Sol-gel processes are used extensively in silicate processing and find various applications elsewhere, variously providing high purity, mild chemical synthesis conditions, stoichiometric control, homogeneous doping, porosity and/or high optical quality.[7] There are reports of sol-gel production of perovskite titanate thin films using spin-coating[8–10] or dip-coating[3,11–13] with sols typically stabilized by acetylacetonate, acetate and methoxyethanol. Film quality is often not discussed in detail in the literature, but volume contraction of the

coating during drying can create internal stresses which cause cracking and pinholes (cracks that cannot propagate due to the film thickness being lower than the critical stress intensity).[14,15]

The film porosity is a critical factor for the production of dielectric thin films for applications such as capacitive devices. If the film is porous, electrode deposition techniques such as thermal evaporation or sputtered electrodes can result in electrical short circuits. No account is usually taken of porosity when calculating relative permittivity values and the permittivities measured in standard experiments using solid samples and metal contacts are an average across the film as a whole.[16] Multiple dipping and annealing steps have been employed to fill in porosity in sol-gel $BaTiO_3$ films, and this process allowed electrical properties to be measured.[11] A review of the literature (SI, Table S1) shows that when $BaTiO_3$ films are made by sol-gel deposition (whether spin- or dip-coating), electrical measurements are only reported on films made with multiple coatings.[3,9–11,17–20]

Herein a sol-gel dip-coating method to produce $BaTiO_3$ thin films on platinum is optimized to remove pinholes and cracks. These single dip films still short-circuited when contacted and multiple dipping steps were used to achieve solid state impedance measurements. A new approach using electrochemical impedance in combination with optical and electron microscopy has then been used to improve understanding of the porosity of the films, allowing the relative permittivity of the $BaTiO_3$ itself to be assessed.

Experimental

All the reagents were used without further purification. 2-Methoxyethanol (99.8%), acetylacetonate (>99%), titanium isopropoxide (97%) and barium acetate (99%) were purchased from Sigma Aldrich and used as received. Glacial acetic acid (>99%) and potassium sulphate (99%) were purchased from Fisher Scientific. Deionized water was produced with a Purelab Options, ELGA LA620 deionizer.

The preparation of $BaTiO_3$ precursor sols was based on a previous report (SI, Fig. S1).[13] $Ti(O^iPr)_4$ (2.618 g, 9.21 mmol) was added to a mixture of methoxyethanol (23.505 g, 309 mmol) and acetylacetone (1.508 g, 15.6 mmol) under N_2 in a dry bottle. In a separate bottle $Ba(OAc)_2$ (2.353 g, 9.21 mmol) was dissolved by stirring in concentrated acetic acid (15 mL, 262 mmol), then when cooled to room temperature H_2O (1-4 mL, 55.5-222 mmol) was added. The $Ba(OAc)_2$ solution was added dropwise to the $Ti(O^iPr)_4$ solution under a N_2 flow. The sol was then sealed in the bottle and allowed to stir at 250 or 1000 rpm over periods ranging from 1 to 14 days depending on water and acetic acid content.

Sols were deposited onto dry 90 nm Pt-coated Si(100) substrates (20 x 30 mm; Ti adhesion layer; ECS Partners Southampton, cleaned by sonicating for 15 minutes each in acetone, ethanol, IPA and deionized water). Substrates were dipped into the sol at a 30 mm s^{-1} immersion speed, held for 30 s, and then withdrawn at 40 mm s^{-1} and left to dry for 10 minutes (NIMA Technology 5.20 dip-coater). The films were then placed into a crucible and fired at 750 °C for 40 minutes (ramp rate of 1 °C min^{-1} and cooling at 5 °C min^{-1}).

Grazing incidence X-ray diffraction was collected using a Rigaku Smartlab diffractometer with a parallel beam of Cu-K_α X-rays, incident angle of 1° and a DTex250 1D detector. Rietveld refinement was carried out using the Rigaku PDXL2 package. Scanning electron microscopy (SEM) and energy dispersive X-ray spectrometry (EDS) were performed on a Jeol JSM6500F microscope with an Oxford Instruments INCA x-sights EDS/EDX detector. Optical images were taken on a Nikon Eclipse optical microscope.

Solid state impedance measurements were performed with an Agilent 4294A Precision Impedance Analyser. Gold top electrodes of various diameters (0.4 mm, 0.5 mm, 0.6 mm) were evaporated onto the $BaTiO_3$ thin film. The Pt of the Si/Pt/$BaTiO_3$ substrate was then contacted as the working electrode. The sinusoidal potential was 10 mV, and the measurement frequency was from 1 MHz to 100 Hz. Data was fitted with ZView.

Electrochemical impedance measurements were carried out using a Biologics SP-150 potentiostat. An area of the $BaTiO_3$ thin film was defined by masking the surrounding area and film edges with an insulating medium (nail polish). The $BaTiO_3$ thin film working electrode was then submerged into 0.5 mol dm^{-3} K_2SO_4 (20 mL) with a Pt gauze counter electrode and an $Hg/HgSO_4$ (sat. K_2SO_4) reference electrode. A sinusoidal potential with 10 mV amplitude was applied at frequencies from 1 MHz to 10 mHz. The subsequent Nyquist plots were fitted using ZView (Scribner Associates Inc) to an appropriate equivalent circuit model giving the capacitance and resistance values.

Results and Discussion

Sol-gel $BaTiO_3$ film optimization

The sol recipe used to produce $BaTiO_3$ films was fairly typical of those in the literature, with coordinating solvents and a reaction moderator (acac) used to stabilize the reactive titanium centers. The films were dipped onto Pt-coated silicon wafer. Grazing incidence XRD of the films fired at 750, 800, 850 and 900 °C (Fig. 1) showed cubic $BaTiO_3$ with lattice parameters of 4.0060(7), 4.0070(6), 4.0057(8) and 4.001(3) Å, respectively. A typical literature value is 4.014 Å.[21] The crystallite sizes were measured using the Halder-Wagner method[22] in the PDXL software as 132 $\pm$ 11 Å across all temperatures, with no obvious trend with firing temperature.

However, at the higher annealing temperatures a $Ba_2Ti_{13}O_{22}$ impurity was also found in the $BaTiO_3$ films, so the work focused on the phase-pure $BaTiO_3$ films which were annealed at 750 °C.

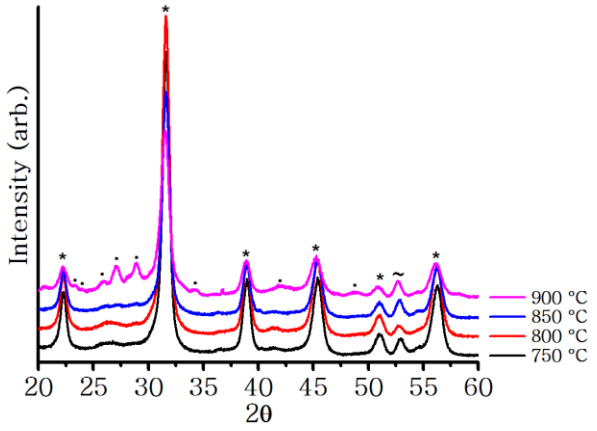

Fig. 1 GIXRD (1° incident angle) of thin films $BaTiO_3$ deposited on Si/Pt substrates and annealed at the indicated temperatures. (*) marks reflections due to cubic $BaTiO_3$, (~) the Pt signals from the substrate and (•) is the $Ba_2Ti_{13}O_{22}$ impurity in the 900 °C sample.

The initial single dip $BaTiO_3$ films contained a high density of pinholes that became visible by eye during drying of the gels and remained visible after the annealing step. Optical microscopy (Fig. 2a) showed some delamination and exposure of the substrate in the center of the pinhole. The delaminated region was shown by SEM (Fig. 2b) to contain a series of short cracks which then open up a little due to the film shrinkage during drying. Presumably these cracks do not propagate across the film thickness as the film thickness is below the critical stress intensity of the material.[14] The EDS maps showed fairly even composition across the flakes of material within the pinholes and a 1:1 ratio of Ti to Ba (Fig. 2c/d) suggesting that pinhole formation is not due to local composition variations. This is supported by microfocus XRD maps across pinholes, where only $BaTiO_3$ and Pt were observed.

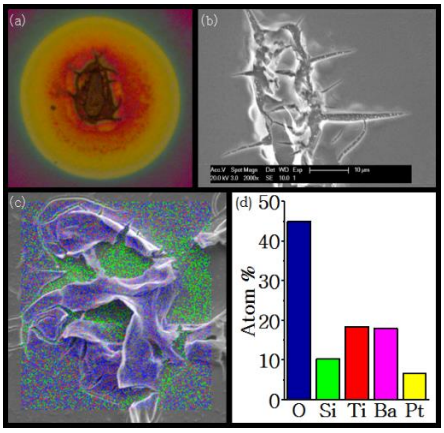

Fig. 2 Optical microscopy (a), SEM image (b), colored EDS map (c, blue, green, red, purple and yellow dots correspond to oxygen, silicon, titanium, barium and platinum respectively) and quantification of the EDS map (d, with values reported in SI, Table S2) of the region of a pinhole in an **unoptimized** single dip $BaTiO_3$ film annealed at 750 °C.

Pinholes are disadvantageous as they can cause electrical shorting and also have a significant influence on capacitance (e.g. in TiO_2 thin films a 1 % surface fraction of pinholes caused a 10 % reduction in capacitance).[23,24] Their formation has been attributed to poor substrate cleaning,[25–27] lack of grain coalescence[28] and solvent effects on the particulate species present within the sol.[29] A number of variations to our glassware and substrate cleaning processes were had no clear effect on the pinhole density. Hence variants in the sol composition and aging were explored with the aim of reducing pinhole formation:

1) The amount of water added to the sol formulation to hydrolyze the titanium isopropoxide was varied. After 1 day of aging the substrate was dipped into the four different sols and then annealed at 750 °C. The film with the lowest number of pinholes (SI, Fig. S2) was produced with 4 mL of H_2O and so this modification was then maintained. The films produced with 4 mL water contained larger particles than those produced at lower water concentration (optical micrographs in SI, Fig. S3) and so this change was attributed to the degree of oligomer development.

2) The length of the sol aging period is also a vital control parameter as the number and size of oligomers formed within the sol will vary with the amount of time over which hydrolysis and polycondensation occur. As the film aging period gradually increased from 1 to 8 days, the pinhole density gradually fell (SI, Fig. S4), with a very low density of pinholes observed with aging periods between 6 and 8 days. With these longer aging periods the films developed small pores that could be observed under the microscope (distinct from the large pinholes described above that are visible to the naked eye), but also increased in overall density (SI, Fig. S3). This is consistent with an increase in sol viscosity.[30] On day 9 the sol had started to gel, and smooth coatings were not achieved due to poor adhesion.

3) The final modification was to the stirring speed during aging, which was increased from 250 to 1000 rpm. This improved reproducibility of the aging periods, and reduced the period taken to produce sols that did not generate pinholes by 2-3 days compared to that at 250 rpm (SI, Fig. S4). At this stirring speed full gelation did not occur even after 9 days, although after 7 days cracks appeared on the film due to high viscosity sols (SI, Fig. S4b).

The faster stirring speed resulted in shorter aging periods to produce pinhole-free films but also reduced the size of the pores that occur in these films (SI, Fig. S3). Further films were produced using 4 mL of water and stirred at 1000 rpm for 3-4 days.

Films produced with multiple dippings

Even after the sol synthesis and aging process had been optimized to avoid pinhole formation, attempts at electrical measurements of the single dip $BaTiO_3$ films always failed. Various methods were used to contact the film top surface (evaporated gold, gallium, gallium-indium eutectic), but short circuits to the platinum film substrate were always observed. Hence even the small pores observed in the microscopy (SI, Fig. S3) are sufficient for these media to penetrate the film. As noted in the introduction, multiple dippings have been claimed to fill in the pores and allow electrical measurement,[11] and in all cases where electrical properties have been reported multiple coating cycles have been employed (ESI, Table S1). Hence films were produced using the optimized dip conditions described above with multiple rounds of dipping and firing. In these films GIXRD (Fig. 3) showed the cubic $BaTiO_3$ to have a constant lattice parameter (4.008 +/- 0.003 Å) and crystallite size (160 +/- 20 Å), but also a minor hexagonal $BaTiO_3$ component. Pt substrate signals were obscured by these thicker films.

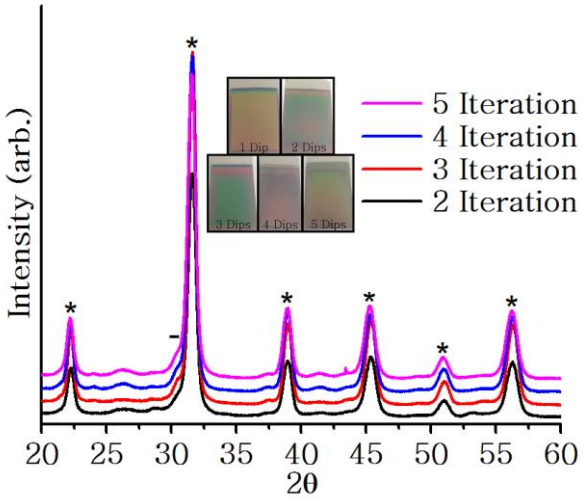

Fig. 3 GIXRD (1° incident angle) of $BaTiO_3$ films deposited on Si/Pt substrates and annealed at 750 °C. (*) marks reflections due to cubic $BaTiO_3$ and (-) the hexagonal $BaTiO_3$. (JCPDS card number 01-076-0738). The inset shows the smooth, pinhole-free films.

The films were smooth to the eye, but under the optical microscope changes to the microstructure were observed (Fig. 4). Over the first three layers of $BaTiO_3$ deposited the pores became smaller but were more numerous. In layer 4 cracks started to appear, and in layer 5 these had propagated to a network of narrow cracks leaving ~5 µm $BaTiO_3$ islands. The film thicknesses progressively increased from 300 nm with 1 dip and anneal cycle, to 550, 600, 930 and 1250 nm with 2, 3, 4 or 5 cycles (respectively). The cross-sectional SEM images (SI, Fig. S5) also showed further evidence of the porosity present between the $BaTiO_3$ grains, which did not appear to have been mitigated by the multiple dipping process.

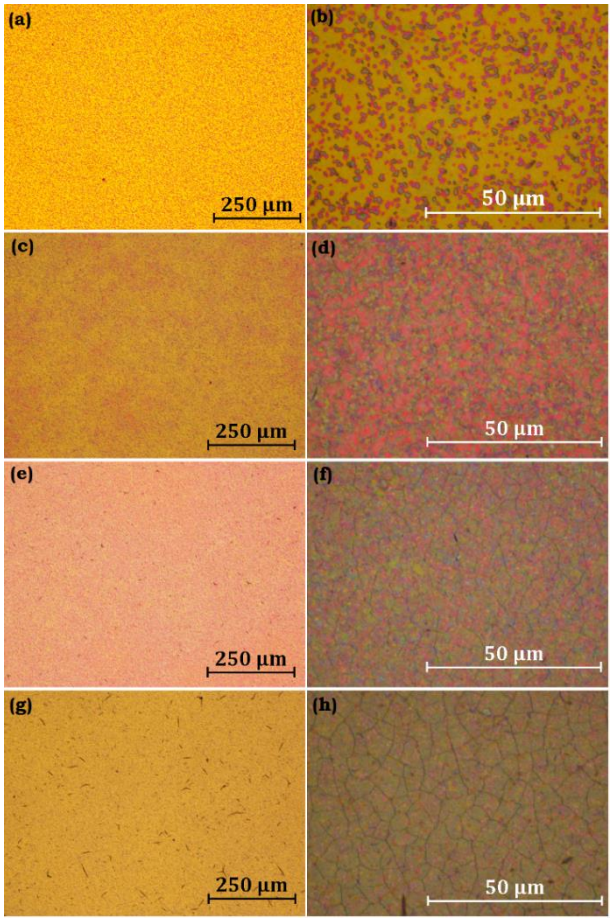

Fig. 4 Optical micrographs (left 10×, right 100×) of $BaTiO_3$ films produced using multiple dip and anneal (750 °C) cycles: (a) and (b) 2 layers ; (c) and (d) 3 layers; (e) and (f) 4 layers; (g) and (h) 5 layers.

Solid state impedance measurements

Single dip films suffered from short circuits when top contacts were applied due to the metal penetrating through the pores. The most continuous $BaTiO_3$ films produced in this study were with 2 or 3 dip and anneal cycles, and with further cycles cracking of the films started to develop. Solid state impedance measurements were focused on the films produced with 3 coating cycles. Gold was evaporated onto the surface of one of these films using a mask with multiple contact diameters (0.420 mm, 0.515 mm and 0.615 mm: SI, Fig. S6). The gold contacts were used as the top contact and the Pt substrate as the bottom contact. Impedance spectroscopy was then carried with a frequency range of 1 MHz to 100 Hz and an amplitude of 10 mV on 3 gold pads of each size. The Nyquist and Bode plots (Fig. 5) show a capacitive response consistent with an equivalent circuit of a resistor and a constant phase element in series. The phase angle was just below 90° throughout the frequency range, the modulus gradient was -0.99 and the magnitude of the capacitance scaled accordingly with pad area. The electrical response was highly reproducible across each pad area. The data were fitted to an

equivalent circuit consisting of a resistor and a constant phase element in series (SI, Fig. S7). Using the parallel plate equation ($C = A\varepsilon\varepsilon_0/d$ where C is capacitance in F, A is pad area in m^2, ε_0 is the permittivity of free space in m^{-3} kg^{-1} s^4 A^2, ε is the relative permittivity of the film and d is its thickness in m) the relative permittivity of the films in each of these regions was then calculated. These were remarkably consistent (SI, Table S3), with an average value of 290 and all measurements between 270 and 299 (~0.5 kHz).

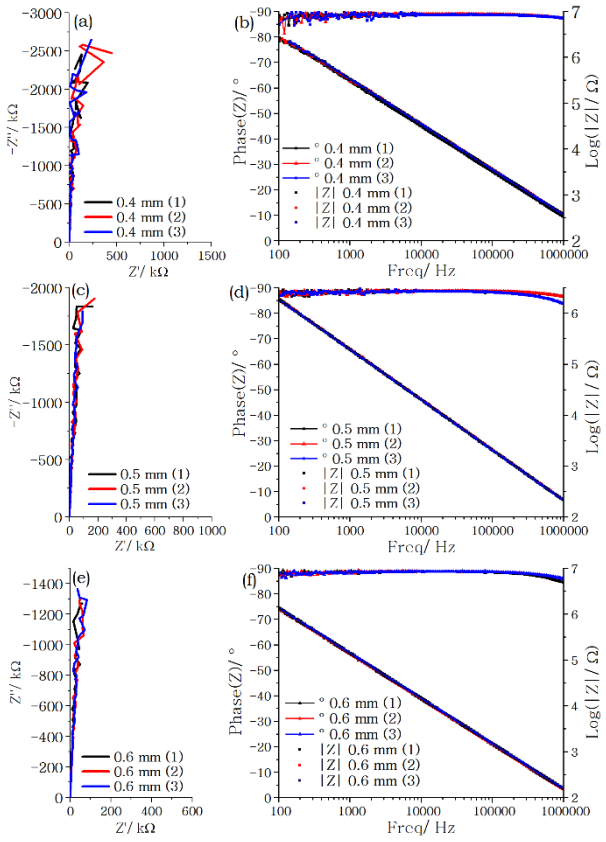

Fig. 5 Nyquist (left) and Bode (right) plots of the solid state impedance data for a $BaTiO_3$ thin film produced by dipping and annealing at 750 °C 3 times: (a) and (b) 0.4 mm; (c) and (d) 0.5 mm; (e) and (f) 0.6 mm diameter contact area. Each experiment was performed on three gold pads of the same diameter to confirm reproducibility (The fittings are shown in SI, Fig. S7).

Electrochemical impedance measurements

Multiple sol-gel coating cycles have previously been reported to fill in the pores in $BaTiO_3$ films and hence allow the solid state impedance to be measured.[11] However, Fig. 4 indicates that some porosity is present even in the films that have been coated multiple times. Cyclic voltammograms of films produced with 1, 2 or 3 dip and anneal cycles all showed the same features typical of platinum electrochemistry. Fig. 6 shows characteristic hydrogen adsorption (H_{ads}) and hydrogen desorption (H_{des}) peaks in the potential range between -0.6 V and -0.4 V.[31]

Note that the current densities are similar after 1, 2 or 3 coating cycles, suggesting that a similar area of the platinum surface is accessible to the electrolyte in each case.

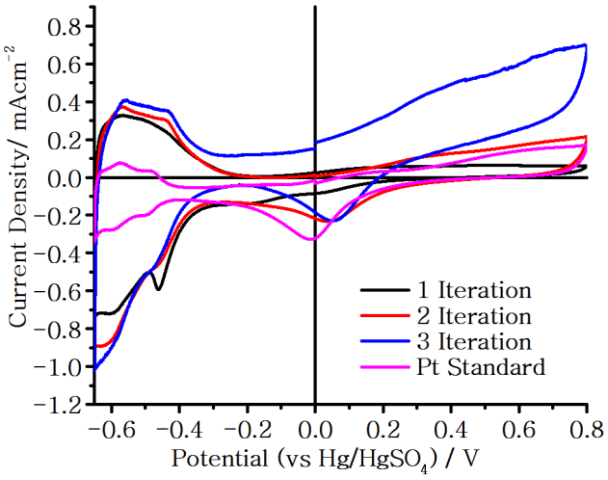

Fig. 6 Cyclic voltammograms of $BaTiO_3$ thin films produced on a Si/Pt substrate with 1, 2 or 3 cycles of dipping into a sol followed by firing at 750 °C, and of a blank Si/Pt substrate. 1 × 1 cm regions were defined using nail polish, the scan rate was 100 mV s^{-1}, a Pt gauze counter electrode and a $Hg/HgSO_4$ reference electrode were used with a non- aerated 1 mol dm^{-3} H_2SO_4 electrolyte.

An electrochemical impedance study was undertaken with the aim of ascertaining how large an effect the porosity has on the capacitance. A comparison between the Pt film substrate and the substrate with a $BaTiO_3$ thin film produced with a single dip and anneal cycle is shown in Fig. 7. Unsurprisingly the bare substrate shows a much lower charge transfer resistance (smaller semicircle in the area normalized Nyquist plot) than the resistive $BaTiO_3$ film. The Bode plots (Fig. 8) show purely resistive behavior at high frequencies due to the solution resistance, and mainly capacitive behavior from 0.1 to 1000 Hz. At low frequency the response goes back to a resistive behavior modelling the film resistance and the solution resistance. The Bode plots for the bare substrate and the film are almost identical, with only a shift along the frequency axis resulting from the resistive component of the $BaTiO_3$ film.

A porous dielectric film is expected to exhibit two parallel impedances associated with transport through the dielectric and the pores. The dielectric part is expected to contain parallel dielectric capacitance and resistance components, whilst the pores should exhibit a double layer capacitance from the platinum surface in series with a pore resistance (SI, Fig. S8). A series of films that had been dipped and annealed between 1 and 5 times were studied with different areas of film exposed to the electrolyte. Nyquist and Bode plots for a series of samples with nominally increasing deposit thicknesses are shown in SI, Fig. S8. The Bode plots all show a linear slope of -1 in modulus and a constant phase of almost 90° from about 1 Hz- kHz, signifying a capacitance ($-1/2\pi f Z''$) on the order of 100 µF and scaling with the sample area. At

frequencies below 1 Hz a lowering of both the phase and modulus suggests a parallel “leakage” resistance in the range of MΩ that can be attributed to redox behavior of impurities such as oxygen in solution. At frequencies higher than 100 Hz a decrease of the phase to almost zero, coinciding with a levelling off of the impedance to constant values of just a few ohms indicates that corresponds well to the estimated series resistance of the electrolyte. The Nyquist plots only show partial arcs from near the origin to the low frequency parallel resistance, scaling inversely with the sample area. Therefore we conclude that the effects of a complex porosity prevent a resolution of the capacitance into C_{dl} and C_D, and the equivalent circuit is effectively reduced to that shown in Fig. 7, where the capacitances are effectively placed in parallel across the same leakage resistor, and the solution resistance is in series with all other components. The data are provided in SI, Fig. S9, with fits shown in SI, Figs. S10-S14 and the fitted parameters in SI, Table S4. Capacitance values varied between 6 and 11 µF cm^{-2}, with similar values throughout and no obvious trend in the values (Fig. 8). An obvious conclusion from these data is that the exposed Pt surface area is similar in all films, hence that pores are not filled in during multiple coating cycles. The ability to measure solid state impedance on such samples must be due to increasing thickness of the films and increasing tortuosity of the pores, resulting in a lower tendency for the evaporated gold, or other contact material, to penetrate to the substrate surface.

Discussion

The relative permittivity of the $BaTiO_3$ films of 290 that was derived from the solid state impedance is significantly higher than that of air (relative permittivity = 1), and so it is reasonable to assume that the pores in the films contribute a negligible amount to this value. The Pt double layer capacitance determined by fitting the data in Fig. 7 was 34.8 µF cm^{-2}, significantly higher than the overall film capacitance determined from Fig. 6 of 0.43 µF cm^{-2}. The capacitance of the $BaTiO_3$ films measured by electrochemical impedance spectroscopy, of ~8 µF cm^{-2}, shows a mixture of Pt double layer capacitance due to electrolyte ingress through the pores and capacitance due to the $BaTiO_3$ film. Considering both types of impedance data together, it is possible to consider the relative contributions of these two capacitances in the electrochemical impedance and hence to evaluate the effect of the porosity on the relative permittivity of the films.

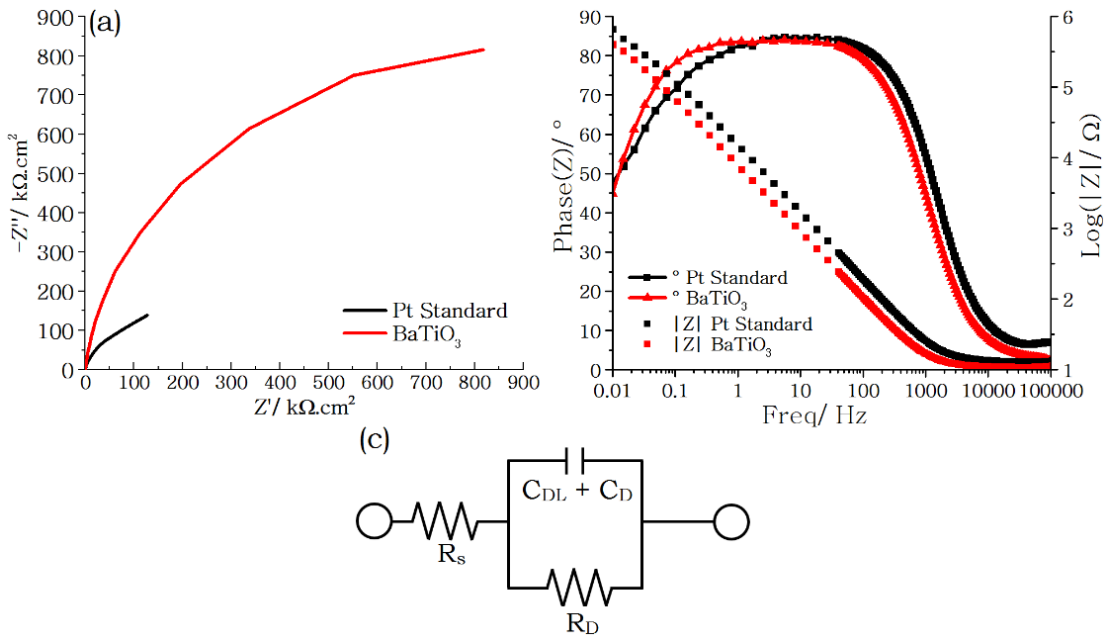

Fig. 7 Nyquist (left) and Bode (right) plots of the electrochemical impedance data for a Pt film substrate and a $BaTiO_3$ thin film produced by dipping and annealing at 750 °C. Data were collected in 0.5 mol dm^{-3} K_2SO_4 (20 mL) with a Pt gauze counter electrode and a $Hg/HgSO_4$ (sat. K_2SO_4) reference electrode. A sinusoidal potential with 10 mV amplitude was applied at frequencies from 0.1 MHz to 10 mHz. (a) is a Nyquist plot using data normalized to the exposed surface area of the substrate or film, (b) is a Bode plot without this normalization and (c) is the equivalent circuit used in data fitting where R_s is uncompensated solution resistance, C_{DL} is double layer capacitance, C_D is dielectric capacitance and R_D is dielectric resistance (pore resistance was discounted).

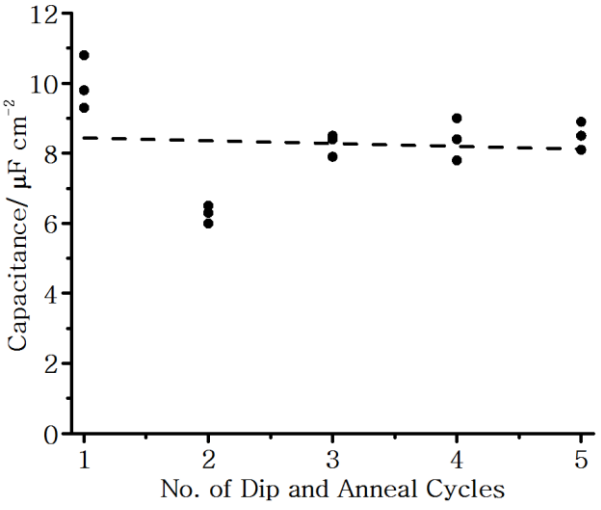

Fig. 8 Variation in area normalized capacitance of $BaTiO_3$ films produced by dipping and annealing at 750 °C 1 to 5 times and each measured using 3 different areas exposed to the electrolyte. The broken line is a guide to the eye.

For the 3-dip films, where we have overall film capacitance data from the solid state impedance, subtracting the overall film capacitance (0.43 μF cm^{-2}) from the electrochemical capacitance (8.26 μF cm^{-2}) provides a double layer capacitance contribution of 7.83 μF cm^{-2}. Dividing this value by the Pt double layer capacitance of a bare Pt film (34.8 μF cm^{-2}) yields an overall pore area of 22.5% of the film surface. This means that the $BaTiO_3$ measured in the solid state impedance only covered 77.5% of the surface, and the relative permittivity of the $BaTiO_3$ itself is higher than that of the film overall, with a value of around 374. Hence if sol-gel coating processes could be refined to avoid all porosity an increase in permittivity of the films of around 29% would be feasible.

Conclusions

Sol-gel $BaTiO_3$ films have been optimized to minimize cracks and pinholes by modifying the water content, aging time and stirring speed during aging. The resultant films are optically smooth and continuous, but do have a significant degree of porosity. After multiple cycles of coating and annealing it was possible to measure an overall film permittivity. These films were found to retain significant porosity, and electrochemical impedance spectroscopy was demonstrated to be a useful technique in such systems to probe the impedance associated with both the pores and the film material. This approach could be powerful in evaluating the effect of porosity on the properties of electroceramic films and in optimizing deposition processes to minimize porosity effects.

Acknowledgements

The authors thank EPSRC for a CASE award to JW (EP/M508147/1) and for funding the Smartlab diffractometer (EP/K00509X/1 and EP/K009877/1).

References

(1) Lian, L.; Sottos, N. R. Effects of Thickness on the Piezoelectric and Dielectric Properties of Lead Zirconate Titanate Thin Films. *J. Appl. Phys.* **2011**, *87*, 3941–3949.

(2) Pontes, F. M.; Lee, E. J. H.; Leite, E. R.; Longo, E. High Dielectric Constant of SrTiO3 Thin Films. *J. Mater. Sci.* **2000**, *35*, 4783–4787.

(3) Kumazawa, H.; Masuda, K. Fabrication of Barium Titanate Thin Films with a High Dielectric Constant by a Sol ± Gel Technique. *Thin Solid Films* **1999**, *353*, 144–148.

(4) Basceri, C.; Streiffer, S. K.; Kingon, A. I.; Waser, R. The Dielectric Response as a Function of Temperature and Film Thickness of Fiber-Textured (Ba,Sr)TiO3 Thin Films Grown by Chemical Vapor Deposition. *J. Appl. Phys.* **1997**, *82* (5), 2497–2504.

(5) Guo, Y.; Batra, S.; Chen, Y.; Wang, E.; Cakmak, M. Roll to Roll Electric Field "Z" Alignment of Nanoparticles from Polymer Solutions for Manufacturing Multifunctional Capacitor Films. *ACS Appl. Mater. Interfaces* **2016**, *8* (28), 18471–18480.

(6) Brennecka, G. L.; Ihlefeld, J. F.; Maria, J. P.; Tuttle, B. A.; Clem, P. G. Processing Technologies for High-Permittivity Thin Films in Capacitor Applications. *J. Am. Ceram. Soc.* **2010**, *93* (12), 3935–3954.

(7) Blum, J. B.; Gurkovich, S. R. Sol-Gel-Derived PbTiO3. *J. Mater. Sci.* **1985**, *20* (12), 4479–4483.

(8) Adikary, S. .; Chan, H. L. . Ferroelectric and Dielectric Properties of Sol–gel Derived BaxSr1−xTiO3 Thin Films. *Thin Solid Films* **2003**, *424* (1), 70–74.

(9) Sharma, H. B.; Mansingh, A. Phase Transition in Sol-Gel-Derived Barium Titanate Thin Films. *J. Phys. D. Appl. Phys.* **1998**, *31* (13), 1527–1533.

(10) Lee, B.; Zhang, J. Preparation, Structure Evolution and Dielectric Properties of BaTiO3 Thin Films and Powders by an Aqueous Sol–gel Process. *Thin Solid Films* **2001**, *388* (1–2), 107–113.

(11) Hayashi, T.; Ohji, N.; Hirohara, K.; Fukunaga, T.; Maiwa, H. Preparation and Properties of Ferroelectric BaTiO 3 Thin Films by Sol-Gel Process. *Jpn. J. Appl. Phys.* **1993**, *32* (Part 1, No. 9B), 4092–4094.

(12) Mahmoodi, N.; Vaezi, M. R.; Kazemzadeh, A. Preparation of Stable Sol and Free-Cracks Thin Film of Barium Titanate via Sol-Gel Dip Coating Method. *J. Ceram. Process. Res.* **2014**, *15* (5), 312–315.

(13) Al-Arjan, W. S.; Algaradah, M. M. F.; Brewer, J.; Hector, A. L. Sol–gel Preparation of Well-Adhered Films and Long Range Ordered Inverse Opal Films of BaTiO3 and Bi2Ti2O7. *Mater. Res. Bull.* **2016**, *74*, 234–240.

(14) Thouless, M. D. Decohesion of Films with Axisymmetric Geometries. *Acta Metall.* **1988**, *36* (12), 3131–3135.

(15) Wang, D.; Bierwagen, G. P. Sol-Gel Coatings on Metals for Corrosion Protection. *Prog. Org. Coatings* **2009**, *64* (4), 327–338.

(16) Kamalasanan, M. N.; Kumar, N. D.; Chandra, S. Dielectric and Ferroelectric Properties of BaTiO3 Thin Films Grown by the Sol-Gel Process. *J. Appl. Phys.* **1993**, *74*, 5679–5686.

(17) Huang, L.; Chen, Z.; Wilson, J. D.; Banerjee, S.; Robinson, R. D.; Herman, I. P.; Laibowitz, R.; O'Brien, S. Barium Titanate Nanocrystals and Nanocrystal Thin Films: Synthesis, Ferroelectricity, and Dielectric Properties. *J. Appl. Phys.* **2006**, *100* (3), 34316.

(18) Hayashi, T.; Oji, N.; Maiwa, H. Film Thickness Dependence of Dielectric Properties of B a T I O 3 Thin Films Prepared by Sol-Gel Method. *Jpn. J. Appl. Phys.* **1994**, *33* (Part 1, No. 9B), 5277–5280.

(19) Sharma, H. B.; Sarma, H. N. K.; Mansingh, A. Ferroelectric and Dielectric Properties of Sol-Gel Processed Barium Titanate Ceramics and Thin Films. *J. Mater. Sci.* **1999**, *34*, 1385–1390.

(20) Kamalasanan, M. N.; Kumar, N. D.; Chandra, S. Dielectric and Ferroelectric Properties of BaTiO3 Thin Films Grown by the Sol-Gel Process. *J. Appl. Phys.* **1993**, *74* (9), 5679–5686.

(21) Yen, F.-S.; Hsiang, H.-I.; Chang, Y.-H. Cubic to Tetragonal Phase Transformation of Ultrafine BaTiO3 Crystallites at Room Temperature. *Jpn. J. Appl. Phys.* **1995**, *34* (Part 1, No. 11), 6149–6155.

(22) Halder, N. C.; Wagner, C. N. J. Separation of Particle Size and Lattice Strain in Integral Breadth Measurements. *Acta Crystallogr.* **1966**, *20* (2), 312–313.

(23) van de Krol, R. Mott-Schottky Analysis of Nanometer-Scale Thin-Film Anatase TiO[sub 2]. *J. Electrochem. Soc.* **1997**, *144* (5), 1723.

(24) Xu, M.; Feng, J.; Ou, X.-L.; Zhang, Z.-Y.; Zhang, Y.-F.; Wang, H.-Y.; Sun, H.-B. Surface Passivation of Perovskite Film by Small Molecule Infiltration for Improved Efficiency of Perovskite Solar Cells. *IEEE Photonics J.* **2016**, *8* (5), 1–7.

(25) Lee, H.-C.; Park, O. O. Round Pinholes in Indium-Tin-Oxide Thin Films on the Glass Substrates: A Taguchi Method Analysis and Theoretical Approach to Their Origins. *Vacuum* **2004**, *72* (4), 411–418.

(26) Lisco, F.; Abbas, A.; Maniscalco, B.; Kaminski, P. M.; Losurdo, M.; Bass, K.; Claudio, G.; Walls, J. M. Pinhole Free Thin Film CdS Deposited by Chemical Bath Using a Substrate Reactive Plasma Treatment. *J. Renew. Sustain. Energy* **2014**, *6* (1), 11202.

(27) Lee, S. M.; Cahill, D. G. Heat Transport in Thin Dielectric Films. *J. Appl. Phys.* **1997**, *81* (6), 2590–2595.

(28) Tashkandi, M. A.; Sampath, W. S. Morphology of CdS Thin Films: Pinholes and Their Effect on Open Circuit Voltage in CdS/CdTe Solar Cells. In *2011 37th IEEE Photovoltaic Specialists Conference*; IEEE, 2011; pp 001700–001704.

(29) Chen, H.-S.; Kumar, R. V. Sol–gel TiO2 in Self-Organization Process: Growth, Ripening and Sintering. *RSC Adv.* **2012**, *2* (6), 2294.

(30) Cairncross, R. A.; Schunk, P.; Chen, K. S.; Prakash, S. S.; Samuel, J.; Hurd, A.; Brinker, C. J. Pore Evolution and Solvent Transport During Drying of Gelled Sol-Gel Coatings: Predicting "Spr1Ngback"*. *Dry. Technol.* **1997**, *15* (6–8), 1815–1825.

(31) Daubinger, P.; Kieninger, J.; Unmüssig, T.; Urban, G. A. Electrochemical Characteristics of Nanostructured Platinum Electrodes – a Cyclic Voltammetry Study. *Phys. Chem. Chem. Phys.* **2014**, *16* (18), 8392–8399.